A Procedure to Correct Airborne Doppler Radar Data for Navigation Errors Using the Echo Returned from the Earth's Surface

JACQUES TESTUD

Centre d'etudes des Environnements Terrestre et Planetaires (CETP) CNET, Issy-Les-Moulineaux, France

PETER H. HILDEBRAND AND WEN-CHAU LEE

National Center for Atmospheric Research, Boulder, Colorado*

(Manuscript received 12 May 1994, in final form 1 February 1995)

ABSTRACT

The development of airborne Doppler radars for atmospheric sciences research has vastly improved the ability to measure atmospheric storms. This paper addresses a new technique for improving airborne Doppler radar data quality. Assuming the earth's surface is flat and still, the technique uses the airborne radar measurements of the earth's surface reflectivity and velocity to correct for errors in navigation and radar pointing angles.

The methodology makes use of the helical scanning adopted in the existing systems onboard the two National Oceanic and Atmospheric Administration P3 aircraft and on the National Center for Atmospheric Research Electra aircraft (ELDORA/ASTRAIA radar). On the basis of a scan-by-scan analysis, it is shown that this methodology has the potential to retrieve most of the navigation errors, including errors in aircraft altitude, aircraft speed and drift, aircraft vertical velocity, aircraft pitch and roll, radar ranging error, and error in antenna spin angle. The methodology is demonstrated using a dataset obtained from ELDORA/ASTRAIA during the Tropical Ocean Global Atmosphere Coupled Ocean–Atmosphere Response Experiment. Analysis of these data shows it is possible to systematically correct for the navigation errors from a large dataset using a single set of corrections to the data.

1. Introduction

Correct navigation of airborne weather radar data with respect to the earth is a critical aspect of producing correct and usable data. To meet the scientific requirements concerning data location and to correct radial velocities for aircraft motion, the aircraft trajectory and velocity and the radar beam-pointing angles must be known with great accuracy with respect to the ground. For this purpose, the systematic detection of the intense echo returned from the earth's surface provides a reference for radial velocity and distance measurements. The objective of this paper is to show how a careful analysis of the radar echoes returned from the earth's surface allows correction of the systematic or random statistical errors in navigation of the radar data. Such errors include antenna mounting errors as well as errors due to the Inertial Navigation System (INS). For the technique developed in this paper, the earth's surface needs to be assumed smooth and geopotentially flat within about one radar range gate length. The measurements used in section 6 are sea surface measurements; however, an extremely flat land surface should also be usable for the technique.

The navigation correction scheme presented in this paper makes use of the dual-beam, helical scanning technique developed for the National Center for Atmospheric Research–Centre d'etudes des Environnements Terrestre et Planetaires, ELDORA/ASTRAIA[1] radar (Hildebrand and Moore 1990; Hildebrand et al. 1994), and has also been adapted to the two National Oceanographic and Atmospheric Administration (NOAA) P3 airborne Doppler radar systems (Hildebrand and Moore 1990; Jorgensen and DuGranrut 1991). The scanning strategy (Fig. 1a) enables the radar to completely scan the volume surrounding the aircraft, obtaining the two (fore and aft) velocity components needed for three-dimensional wind field retrieval. The radar spins about an axis parallel to the

* The National Center for Atmospheric Research is sponsored by the National Science Foundation.

Corresponding author address: Dr. Peter H. Hildebrand, Remote Sensing Facility, NCAR/ATD, P.O. Box 3000, Boulder, CO 80307-3000.

[1] ELDORA/ASTRAIA stands for Electra Doppler radar/analyse stereoscopic par impulsions aeroperte.

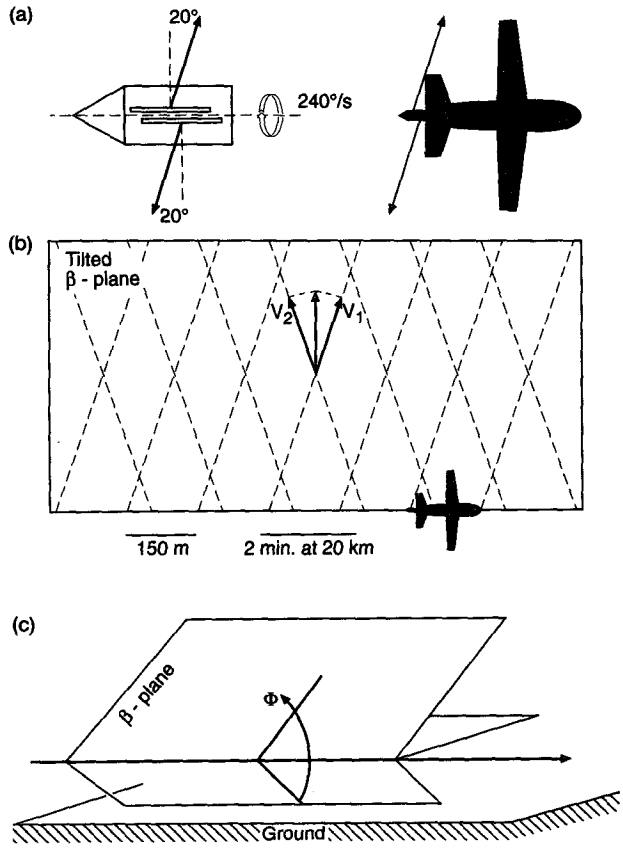

FIG. 1. (a) Fore and aft sampling scheme with ELDORA/ASTRAIA. (b) The data can be viewed as sampled on a β plane with a spin angle ϕ (defined in section 2). (c) At any point of the three-dimensional space, the radar system measures two independent components of air velocity within a β plane (or plane including the aircraft trajectory). The component perpendicular to β plane is not seen and should be determined through integration of the continuity equation.

aircraft's longitudinal axis, with the beams tilted a fixed amount fore and aft of a plane normal to the spin axis.

The implementation of the radars and scanning in each of the three aforementioned airborne Doppler radar systems is somewhat different; however, a common approach can be used to correct the navigation. In ELDORA/ASTRAIA, the ±18.5° fore and aft tilt angles are scanned simultaneously using a dual transmitter–receiver radar system. In the NOAA P3 with the French dual-antenna system, the fore and aft antennas are illuminated using a single transmitter/receiver and a waveguide switch: the fore and aft antennas are typically illuminated for 180° or 360° revolution so as to observe on one side of the aircraft or on both sides. The other NOAA system uses a single antenna with adjustable tilt and creates the fore and aft scans by tilting the antenna fore and aft as the whole system is rotated about the longitudinal spin axis (Jorgensen and DuGranrut 1991).

2. Geometry of the problem

Figure 2 illustrates the geometry of the problem. All circles in Fig. 2a are great circles. The notations can be divided into several groups as follows:

1) General description
   - O is the position of the antenna and the center of a reference sphere.
   - Z is the zenith.
2) Aircraft coordinates
   - C (T) is the intersection of the nose (tail) of the fuselage and the sphere and CT is the antenna spin axis.
   - OB is the projection of OC to the horizon.
   - A is the intersection of the aircraft track velocity and the sphere.
   - D is the vertical with respect to the aircraft.
   - α (arc AB) is the drift angle, or angle from the vertical plane including the antenna spin axis (heading) to the horizontal component of the aircraft velocity (track). The drift is positive if track is more clockwise than the heading (Lee et al. 1994).
   - β (arc BC) is the pitch of the antenna spin axis (positive up).
3) Absolute beam coordinates
   - E is the intersection of the radar beam and the sphere.
   - EL (arc EF) is the elevation angle of the beam with respect to the horizontal plane.
   - Ψ (arc EA) is the angle between the beam and the horizontal component of aircraft velocity.
4) Beam coordinates relative to the aircraft
   - θ (arc DE) is the tilt angle from the plane perpendicular to spin axis to the beam, positive when antenna is pointing fore, negative when antenna is pointing aft.
   - ϕ (angle BCE) is the spin angle (the sum of the rotation angle of the antenna given by the encoder and the roll of the aircraft). Both the spin angle and the rotation angle are measured clockwise when looking forward. Zero rotation angle corresponds to the antenna pointed downward with respect to the airframe while zero ϕ corresponds to a beam pointed toward nadir).
   - A_z (arc BF) is the azimuth of the beam relative to the heading (positive clockwise).

Spherical trigonometry provides the following dependence of Ψ, EL, and A_z as a function of α, β, θ, and

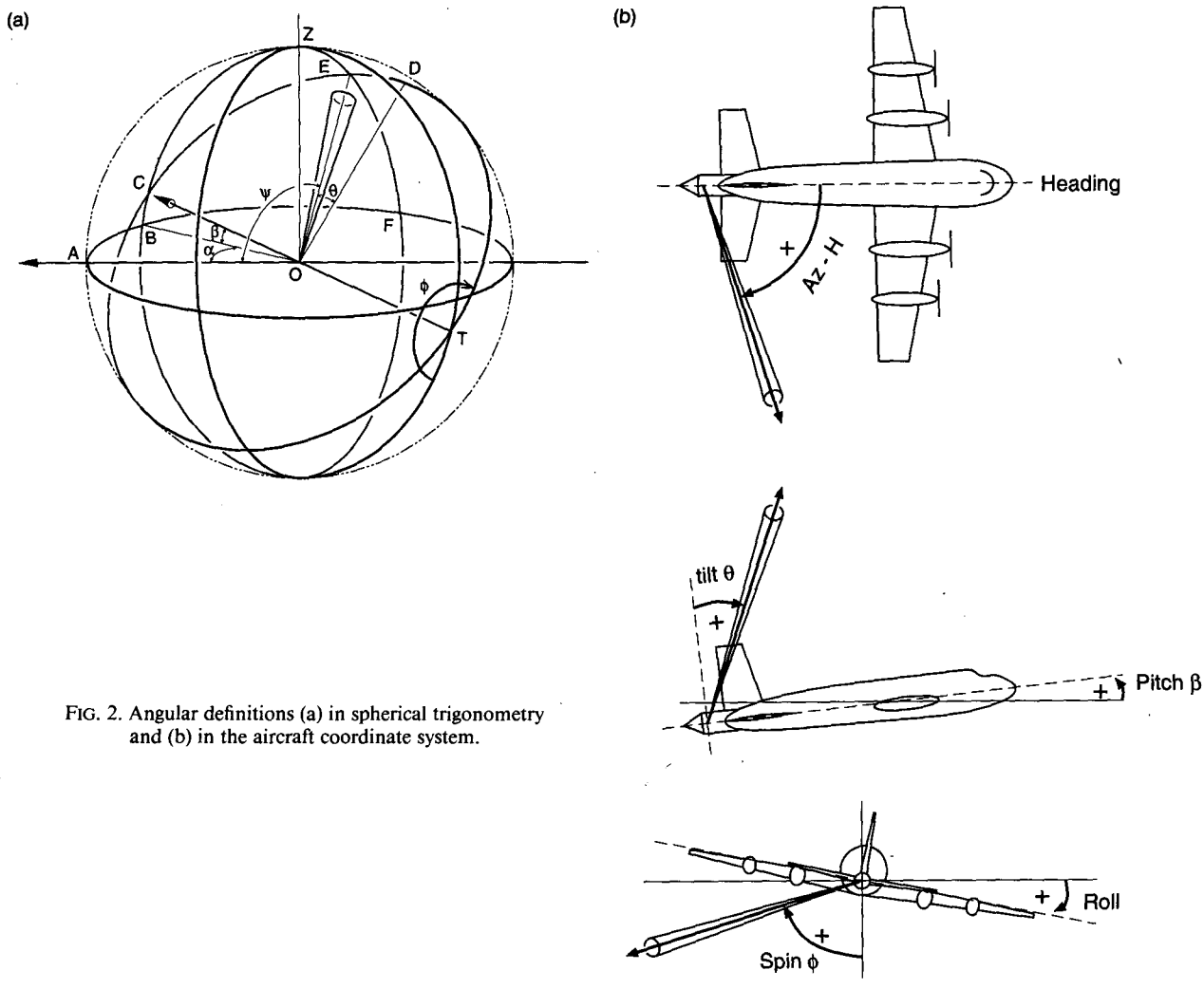

FIG. 2. Angular definitions (a) in spherical trigonometry and (b) in the aircraft coordinate system.

ϕ (the derivations are detailed in appendix A for interested readers):

$$\cos A_z = \frac{\sin\theta - \text{sinEL}\,\sin\beta}{\text{cosEL}\,\cos\beta} \quad (1)$$

$$\text{sinEL} = \sin\theta\,\sin\beta - \cos\theta\,\cos\beta\,\cos\phi \quad (2)$$

$$\cos\Psi = \cos\alpha\,\cos\beta\,\sin\theta + \cos\alpha\,\sin\beta\,\cos\theta\,\cos\phi - \sin\alpha\,\cos\theta\,\sin\phi. \quad (3)$$

3. Surface echo detection

When looking toward the ground at an incidence off from down, we may define the antenna footprint as the projection of the beam (we consider here only the one-way 3-dB main lobe) over the earth surface (Fig. 3). All the radar range gates intersecting the footprint will be affected by the surface echo, and the energy received in a given gate will be proportional to the portion of the footprint it intersects. The following notation is used:

- H: altitude of the aircraft above the earth surface.
- ϵ: 3-dB cross-beam resolution of the antenna (one way).
- δR: range resolution of the radar.
- R_G: "mean" range of the earth surface along a beam when operating at elevation angle EL.
- N_G: number of contiguous gates affected by the earth surface.

Parameters R_G and N_G may be expressed as[2]:

[2] A more accurate formula taking account of the earth curvature is $R_G = [-H(\text{sinEL})^{-1}]\,[1 + H(2\rho\,\tan^2\text{EL})^{-1}]$, where ρ denotes the earth radius. This formula should be preferred when EL $\leq -40°$.

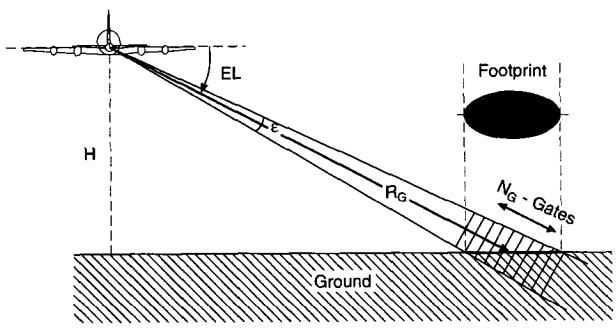

FIG. 3. Range gates affected by the surface echo.

$$R_G = -\frac{H}{\text{sinEL}} \tag{4}$$

$$N_G \approx \frac{R\epsilon}{\delta R \,\text{tanEL}}. \tag{5}$$

Figure 4 displays N_G as a function of ϕ in typical operational conditions for the NOAA P3 tail radar ($\epsilon = 2°$; $\delta R = 75$ m; $H = 5700$ m, $\theta = 22.23°$). To quantitatively measure the surface echo power, all gates intersecting the portion of the footprint away from the center should be deleted for they are negatively biased with respect to the most central gate. It can be shown that if we restrict ourselves to the $N_G/2$ gates closest to center gate, the bias for these gates will never exceed −0.65 dB.

When the radar operates over land, the power of the signal returned from the ground can be higher than that from meteorological targets. Thus, a simple procedure can be used to select the gates affected by the ground clutter: after calculating the expected ground range R_G at which we expect the ground [according to (4)], we select, among the ±20 closest gates to range R_G, the $N_G/2$ gates within 3 dB of highest reflectivity. When operating over the ocean, the surface clutter is often less powerful than the weather echo (which may also be present in reflection) and may be obscured by the presence of moderate or heavy rain in the same resolution cell. Therefore, it is important to collect ocean surface data on a weather echo-free region to avoid contamination of the surface velocity from the weather. It is assumed that the ocean surface clutter velocity, is approximately zero. A test of the Doppler velocity, which should be close to zero if it is surface clutter, can serve to identify these cases. Throughout this paper, it is assumed that any aliasing of the Doppler velocity about the Nyquist velocity has already been removed.

4. Error analysis of the navigation parameters

The uncertainties in the parameters provided by the INS and by the encoder of the antenna pedestal for the ELDORA/ASTRAIA are the following:

Horizontal velocity:	±2 m s^{-1}
Drift angle:	±1°
Aircraft vertical velocity:	±0.15 m s^{-1}
Pitch angle:	±0.05°
Tilt angle:	±0.05°
Roll and/or spin angle:	±0.05°

In addition to these statistical uncertainties there are systematic errors due to various imperfections such as the antenna mounting. Systematic errors of the order of 1° may exist in β, α, ϕ, and θ. The primary goal of the error analyses in this section is to identify the magnitude of uncertainty in these navigation and radar pointing parameters.

a. *Velocity error analysis*

With respect to the reference frame of the aircraft, any fixed target on the earth's surface moves at a velocity opposite to that of the aircraft in the terrestrial frame. In "normal" flight conditions where the aircraft is not submitted to sudden changes in pitch, drift, or roll, we may consider that the radar antenna is moving at the aircraft ground speed. The radar observed surface radial velocity V_G (positive away from the radar) may be expressed as a function of the horizontal and vertical components of aircraft velocity, V_H and W, and of the Ψ and EL as

$$V_G = -V_H \cos\Psi - W \,\text{sinEL} \tag{6}$$

or

$$V_G = -V_H(\cos\beta\cos\alpha\sin\theta + \sin\beta\cos\alpha\cos\theta\cos\phi - \sin\alpha\cos\theta\sin\phi) - W(\sin\theta\sin\beta - \cos\theta\cos\beta\cos\phi). \tag{7}$$

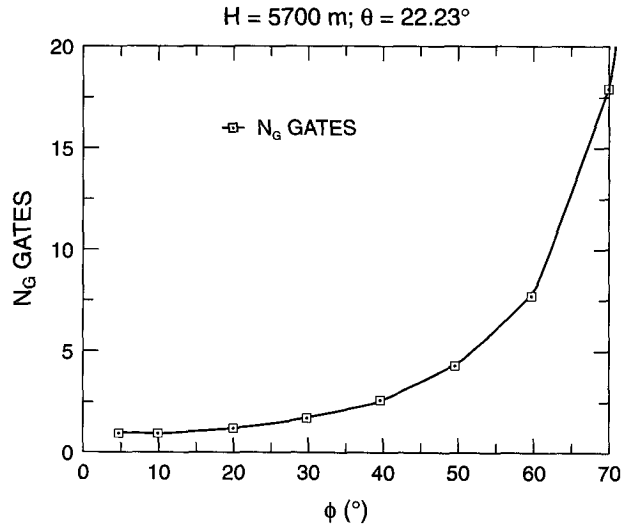

FIG. 4. Numbers of gates affected by the surface echo as a function of the spin angle of the antenna.

All parameters in (7) (except the spin and tilt angles, ϕ and θ) are output parameters of the INS.

Correcting the radar radial velocities for navigation errors involves comparing the measured ground velocities V_G with estimated ground velocities V_{Ge} calculated from (7), using the aircraft navigation parameters, α, β, V_H, and W, from the INS, and the radar pointing angles, θ and ϕ. The difference, $\delta V_G = V_G - V_{Ge}$, is due to the inherent uncertainties in the INS measurement (including biases and drifts of the INS) and the radar mounting errors (fixed biases), plus the radar's statistical sampling error (hopefully, in comparison, small numbers). The residue δV_G can be evaluated as follows:

$$\delta V_G = V_G - V_{Ge} \tag{8}$$

$$= \delta(-V_H \cos\Psi - W \sin\text{EL}). \tag{9}$$

If we assume the pitch angle is small ($\beta \leqslant 2°$) and $W \ll V_H$, then (7) can be used to obtain

$$\begin{aligned}\delta V_G = {} & \cos\theta \cos\phi \delta W \\ & - V_H(\cos\alpha \cos\theta + \sin\alpha \sin\theta \sin\phi)\delta\theta \\ & + V_H \sin\alpha \cos\theta \cos\phi \delta\phi \\ & - V_H \cos\alpha \cos\theta \cos\phi \delta\beta \\ & + V_H(\sin\alpha \sin\theta + \cos\alpha \cos\theta \sin\phi)\delta\alpha \\ & - (\cos\alpha \sin\theta - \sin\alpha \cos\theta \sin\phi)\delta V_H \end{aligned} \tag{10}$$

$$= A + B_1 \sin\phi + B_2 \cos\phi, \tag{11}$$

where

$$\begin{aligned} A = {} & -V_H(\cos\alpha \cos\theta\delta\theta - \sin\alpha \sin\theta\delta\alpha) \\ & - \cos\alpha \sin\theta\delta V_H \end{aligned}$$

$$\begin{aligned} B_1 = {} & -V_H(\sin\alpha \sin\theta\delta\theta - \cos\alpha \cos\theta\delta\alpha) \\ & + \sin\alpha \cos\theta\delta V_H \end{aligned}$$

$$\begin{aligned} B_2 = {} & \cos\theta\delta W \\ & + V_H(\sin\alpha \cos\theta\delta\phi - \cos\alpha \cos\theta\delta\beta). \end{aligned} \tag{12}$$

All the δ quantities are defined as the true value minus the measured value. Therefore, all correction factors obtained in this procedure should be added to their corresponding measured values. In normal flight conditions, the angle α does not exceed a few degrees and (12) may be approximated as

$$\begin{aligned} A &= -V_H \cos\alpha \cos\theta\delta\theta + \sin\theta(V_H \sin\alpha\delta\alpha - \cos\alpha\delta V_H) \\ B_1 &= -V_H \sin\alpha \sin\theta\delta\theta + \cos\theta(V_H \cos\alpha\delta\alpha + \sin\alpha\delta V_H) \\ B_2 &= \cos\theta\delta W - V_H \cos\alpha \cos\theta\delta\beta. \end{aligned} \tag{13}$$

b. Range error analysis

Similar considerations can be applied to radar observations of the range to the earth's surface. Using techniques discussed above, the distance from the radar to the earth's surface R_G can be determined for any beam intersecting the earth's surface as follows:

$$\begin{aligned} R_G &= -\frac{H}{\sin\text{EL}} \\ &= -\frac{H}{\sin\theta \sin\beta - \cos\theta \cos\beta \cos\phi}, \end{aligned} \tag{14}$$

where the negative sign results from EL $\leqslant 0$ for downward beams. Using (2) and assuming a flat earth surface, the estimated range R_{Ge} can be estimated using INS and radar pointing angle:

$$R_{Ge} = -\frac{H_e}{\sin\theta_e \sin\beta_e - \cos\theta_e \cos\beta_e \cos\phi_e}. \tag{15}$$

As was the case in the velocity error or residue, a range error can be calculated from $\delta R_G = R_G - R_{Ge}$, where R_G is the true distance from the radar to the earth surface along a beam. However, in this case, the measured distance from the radar to the earth surface R_R is the gate spacing multiplied by the number of gates in between. Thus, R_G and R_R differ by the range delay of the radar ΔR (a common source of bias in radar measurements), and $R_G = R_R + \Delta R$. The residual error is thus

$$R_R - R_{Ge} = \delta R_G - \Delta R. \tag{16}$$

Differentiating (14) and assuming β is small, δR_G can be approximated as follows:

$$\delta R_G = R_G\left(\frac{\delta H}{H} + \frac{\tan\theta}{\cos\phi}\delta\beta + \tan\theta\delta\theta + \tan\phi\delta\phi\right). \tag{17}$$

Substituting (17) into (16) and multiplying both sides by $\cos^2\phi$, we obtain

$$\begin{aligned} & \cos^2\phi(R_R - R_{Ge}) \\ & = -\frac{\Delta R}{2} + \frac{H \tan\theta}{\cos\theta}\delta\beta + \left(\frac{H\delta\phi}{\cos\theta}\right)\sin\phi \\ & \quad + \left(\frac{\delta H + H \tan\theta\delta\theta}{\cos\theta}\right)\cos\phi - \frac{\Delta R}{2}\cos 2\phi \end{aligned} \tag{18}$$

$$= C + D_1 \sin\phi + D_2 \cos\phi + E \cos 2\phi, \tag{19}$$

where

$$\begin{aligned} C &= -\frac{\Delta R}{2} + \frac{H \tan\theta}{\cos\theta}\delta\beta \\ D_1 &= \frac{H\delta\phi}{\cos\theta} \\ D_2 &= \frac{\delta H + H \tan\theta\delta\theta}{\cos\theta} \\ E &= -\frac{\Delta R}{2}. \end{aligned} \tag{20}$$

As will be illustrated later, the accuracy in determining the surface gate decreases as the beam approaches horizontal due to the 2° beamwidth of the airborne radar antennas. Since the number of gates selected by this procedure increases as EL decreases, those gates influenced by the beam-filling effect outweigh those gates near nadir. To properly weight the data, all gates along a beam are weighted by the inverse of the number of selected gates for that beam (i.e., the average value of those selected gates) so the contribution from each beam is the same. In addition, the $\cos^2\phi$ in the left-hand side of (18) ensures that heavier weights are applied to reliable data ($\phi \sim 0$) and lesser weights are applied to data near the horizon ($\phi \sim \pm\pi/2$).

5. Analysis of the residual radial velocity and of the ranging error of the earth surface

In this section we consider operation of the radar in normal conditions, that is, the aircraft flying along an approximately straight trajectory, at constant level, and in moderate turbulence. In such conditions, we expect that the flight parameters, α, β, γ, V_H, and W will evolve with a characteristic time of the order of a few tens of seconds, that is, much longer than the time of a complete 360° revolution of the antenna (6 s for ELDORA/ASTRAIA, 10 s for the NOAA P3s during TOGA COARE). Hereinafter, we define "scan" as a complete 360° revolution of the antenna from $\phi = -90°$ to $\phi = 270°$. Assuming the approximate stationarity of the flight parameters during each individual scan, the residual radial velocity of the ground δV_G and the ground ranging error $R_R - R_{Ge}$ should vary as a function of ϕ as shown in (11) and (19), and A, B_1, B_2, C, D_1, D_2, and E remain constant at the timescale greater than an individual scan.

For each scan, we select the rays within the range $-80° \leqslant \phi \leqslant 80°$. For these rays, the gates affected by the surface clutter are selected using the procedure described in section 2. Let i be an index numbering all of the selected gates in the scan in question ($i = 1, N$). Each gate i corresponds to a measured residual radial velocity of the ground δV_{Gi} and a range deviation $(R_R - R_{Ge})_i$. In any ray, the number of gates affected by ground varies from 3 to 20 depending on the spin angle ϕ as illustrated in Fig. 4.

a. Determination of A, B_1, and B_2

The A, B_1, and B_2 coefficients may be determined by a least-squares fit; that is, these coefficients are chosen to minimize the quadratic form

$$S = \sum_{\{i\}} (\delta V_{Gi} - A - B_1 \sin\phi - B_2 \cos\phi)^2. \quad (21)$$

Consequently, they should verify

$$\frac{\partial S}{\partial A} = 0, \quad \frac{\partial S}{\partial B_1} = 0, \quad \frac{\partial S}{\partial B_2} = 0 \quad (22)$$

or

$$NA + (\sum_{\{i\}} \sin\phi_i)B_1 + (\sum_{\{i\}} \cos\phi_i)B_2 = \sum_{\{i\}} \delta V_{Gi}$$

$$(\sum_{\{i\}} \sin\phi_i)A + (\sum_{\{i\}} \sin^2\phi_i)B_1 + (\sum_{\{i\}} \sin\phi_i \cos\phi_i)B_2 = \sum_{\{i\}} \delta V_{Gi} \sin\phi_i$$

$$(\sum_{\{i\}} \cos\phi_i)A + (\sum_{\{i\}} \sin\phi_i \cos\phi_i)B_1 + (\sum_{\{i\}} \cos^2\phi_i)B_2 = \sum_{\{i\}} \delta V_{Gi} \cos\phi_i. \quad (23)$$

This linear system with respect to A, B_1, and B_2 can be solved with the following notation:

$$a = N, \quad b = \sum_{\{i\}} \sin^2\phi_i, \quad c = \sum_{\{i\}} \cos^2\phi_i,$$

$$d = \sum_{\{i\}} \sin\phi_i, \quad e = \sum_{\{i\}} \cos\phi_i, \quad f = \sum_{\{i\}} \sin\phi_i\cos\phi_i,$$

$$r = \sum_{\{i\}} \delta V_{Gi}, \quad s = \sum_{\{i\}} \delta V_{Gi} \sin\phi_i,$$

$$t = \sum_{\{i\}} \delta V_{Gi} \cos\phi_i. \quad (24)$$

We obtain

$$\begin{pmatrix} A \\ B_1 \\ B_2 \end{pmatrix} = \frac{1}{\Delta} \begin{pmatrix} bc - f^2 & ef - cd & df - be \\ ef - cd & ac - e^2 & ed - af \\ df - eb & ed - af & ab - d^2 \end{pmatrix} \begin{pmatrix} r \\ s \\ t \end{pmatrix}, \quad (25)$$

with $\Delta = abc + 2def - af^2 - be^2 - cd^2$.

b. Determination of C, D_1, D_2, and E

Similarly, the C, D_1, D_2, and E coefficients may be determined by a least-squares fit (see appendix B) that minimizes the quadratic form

$$S = \sum_{\{i\}} [\cos^2\phi_i (R_R - R_{Ge})_i - C - D_1 \sin\phi_i - D_2 \cos\phi_i - E \cos 2\phi_i]^2. \quad (26)$$

Because of the limited interval in ϕ where data are available (typically $-80° \leqslant \phi \leqslant 80°$, it is not possible to determine accurately the four parameters without a subsidiary condition. In particular, coefficients C, D_2, and E tend to interact with each other. This is because all three define even functions with respect to ϕ, and thus behave similarly about $\phi = 0$. Therefore, various combinations of C, D_2, and E provide fits with a similar standard deviation. Among all these fits, we arbitrarily

choose the one that minimizes the sum of the square of the coefficients involved; that is,

$$T = C^2 + D_2^2 + E^2. \quad (27)$$

The solution of the variational problem defined by (26) under the subsidiary condition (27) is obtained by introduction of a weighting function μ (Courant and Hilbert 1953) and minimization of functional Q defined as

$$Q = S + \mu NT, \quad (28)$$

where N is the number of selected ground gates.

Again, coefficients C, D_1, D_2, and E that minimize Q should verify

$$\frac{\partial Q}{\partial C} = 0, \quad \frac{\partial Q}{\partial D_1} = 0, \quad \frac{\partial Q}{\partial D_2} = 0, \quad \frac{\partial Q}{\partial E} = 0. \quad (29)$$

The corresponding equations are explicitly derived in appendix B. The benefit of introducing the subsidiary condition (27) is to reduce the large fluctuations in C, D_2, and E estimates. But this condition also tends to force the solution to equal values in C, D_2, and E and hence bias the results if one of the coefficients is much larger than the others. However, this effect can be minimized by choosing a small weighting function μ. It turned out that the determination of C, D_1, D_2, and E is, in fact, largely independent on the choice of the weighting function, provided it be chosen below a certain threshold. Practically, we have found that a value of μ between 0.01 and 0.1 provides stable results and $\mu = 0.01$ is used in this paper.

6. Interpretation of the coefficients

For each revolution of the antenna of ELDORA/ASTRAIA or each two revolutions of the P3 antenna, the analysis described in section 5 may be performed for both the fore and aft antenna measurements. For each antenna, we get a set of seven Fourier coefficients related to the navigation, mounting, or radar ranging errors:

$$A = -V_H \cos\alpha \cos\theta\delta\theta + \sin\theta(V_H \sin\alpha\delta\alpha - \cos\alpha\delta V_H)$$

$$B_1 = -V_H \sin\alpha \sin\theta\delta\theta + \cos\theta(V_H \cos\alpha\delta\alpha + \sin\alpha\delta V_H)$$

$$B_2 = \cos\theta\delta W - V_H \cos\alpha \cos\theta\delta\beta$$

$$C = -\frac{\Delta R}{2} + \frac{H \tan\theta}{\cos\theta}\delta\beta$$

$$D_1 = \frac{H\delta\phi}{\cos\theta} \quad D_2 = \frac{\delta H + H \tan\theta\delta\theta}{\cos\theta}$$

$$E = -\frac{\Delta R}{2}. \quad (30)$$

We now discuss how these relations can be inverted to determine the navigation, mounting, and radar ranging errors. In the following, subscript f refers to the fore antenna, and subscript a refers to the aft antenna. It is noted that the analysis provides 14 independent coefficients (seven for each antenna) linearly related to eight navigation or positioning errors ($\delta\alpha$, δV_H, δW, $\delta\theta$, $\delta\beta$, $\delta\phi$, ΔR, δH). To exploit this redundancy of information, and to take account of the respective uncertainty in the determination of A, B_1, B_2 ($\approx$0.1 m s^{-1}) and of the C, D_1, D_2, E ($\approx$10 m), it is particularly useful to estimate some of the eight errors using a variational approach.

a. Radar ranging error

The radar ranging error is determined by the simple relation

$$\Delta R_{af} = -2E_{af}. \quad (31)$$

The radar ranging error is expected to be stable, at least for the duration of a flight. To improve accuracy, this formula can be integrated over the ensemble of the scans sampled during the flight. We may write

$$\langle \Delta R_{af} \rangle = -2\langle E_{af} \rangle, \quad (32)$$

where the angle brackets denote the averaging over an ensemble of scans. If E is determined within $\pm$10 m, the uncertainty in ΔR is $\pm$20 m.

b. Error in the tilt angle

In the ELDORA/ASTRAIA radar, and in the P3 equipped with the French dual-beam antenna, the two antennas are mounted back-to-back on a rigid frame. They are identical and their radiation patterns are known. For each antenna, the pointing angle of the main lobe does not change with time, because it is intrinsically defined by the position of the slots in the waveguides constituting the antenna. We do not expect with these antennas any error in the tilt (θ) angle. There may be an error in the mounting of the rigid frame on the antenna pedestal that may induce systematic errors in the drift (α) and pitch (β) angles, or an error in the roll angle reference that would appear as a bias in the spin (ϕ) angle. Any such errors for the fore and aft antenna would be the same. In the P3 equipped with its original antenna and operated following the fore–aft scanning technique (FAST) (Jorgensen and DuGranrut 1991), there may be additional systematic errors due to a wrong reference for tilt angle.

Any error in the tilt angle should be a systematic error. As said before, this error should be negligible for ELDORA/ASTRAIA and for the P3 radar equipped with the French antenna. For the P3 radar with its original antenna, operating with the FAST methodology, we may establish from the A coefficient in (30) the following estimator:

$$\delta\theta = -\frac{A_f + A_a}{2V_H \cos\alpha \cos\theta_f}. \quad (33)$$

The second term on the right-hand side of the equation tended to cancel between the fore and aft antenna due to the opposite sign of the tilt angle. The above equation may be averaged as

$$\langle\delta\theta\rangle = \left\langle -\frac{A_f + A_a}{2V_H \cos\alpha \cos\theta_f}\right\rangle. \quad (34)$$

With an uncertainty in A of ± 0.1 m s^{-1}, the subsequent uncertainty in $\delta\theta$ would be $\pm 0.07°$, only slightly worse than the corresponding value for the ELDORA/ASTRAIA and the P3 radar with the French antenna ($\delta\theta = \pm 0.05°$).

c. Other navigation errors

We may calculate the errors from the A, B_1, B_2, C, D_1, and D_2 coefficients. However, an alternative approach consists of correcting the dataset for ΔR and $\delta\theta$ errors, then determining a new set of coefficients noted "prime," and related to other errors as

$$A' = \sin\theta(V_H \sin\alpha\delta\alpha - \cos\alpha\delta V_H),$$
$$B'_1 = \cos\theta(V_H \cos\alpha\delta\alpha + \sin\alpha\delta V_H),$$
$$B'_2 = \cos\theta\delta W - V_H \cos\alpha \cos\theta\delta\beta,$$
$$C' = \frac{H\tan\theta}{\cos\theta}\delta\beta, \quad D'_1 = \frac{H\delta\phi}{\cos\theta}, \quad D'_2 = \frac{\delta H}{\cos\theta}. \quad (35)$$

This approach has the advantage of first correcting for the range delay ΔR that can be different between fore and aft radars and the potential bias of the tilt angle $\delta\theta$ for the P3 radar with its original antenna. Then, other sources of errors can be corrected as the residual errors. Experience has shown that the least-squares curve fit on data from either fore or aft antenna alone was unstable because only approximately 160° of the full 360° domain has data. However, we can combine the data from the fore and aft antennas. To do this, we change θ into $-\theta$ (i.e., from the fore to aft antenna), A' and C' change to $-A'$ and $-C'$, respectively, while B'_1, B'_2, D'_1, and D'_2 remain unchanged. Then, if we take the opposite of the aft signal and shift it by 180°, when considering it with the fore signal as a whole, we obtain a 320° sample over the 360° domain (Fig. 5) allowing a more accurate determination of the coefficients.

In the following, A, B_1, B_2, C, D_1, D_2, and E denote the coefficients resulting from a "180°" analysis practiced alternately on a fore and an aft scan, and A', B'_1, B'_2, C', D'_1, and D'_2 denote the coefficients obtained from this combined "360°" analysis.

1) SPIN ANGLE ERROR

The spin angle error consists of the addition of a navigation error of random statistical nature expected to be of a few tenths of a degree at most, and of a systematic mounting error that may reach 1° or 2°. We have

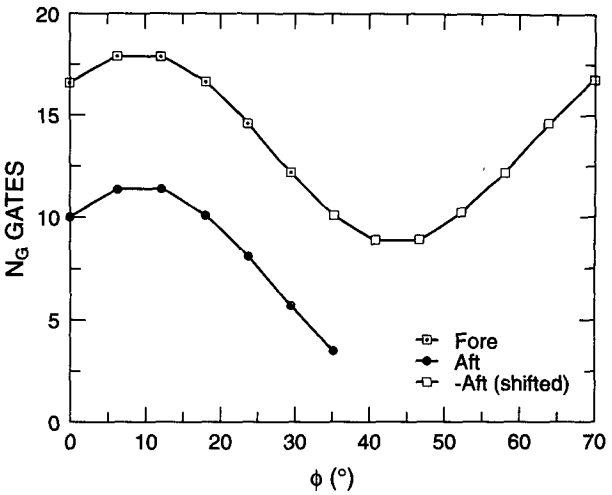

FIG. 5. Simulation of the residual velocity from the surface with the fore antenna ($A' = 1$; $B'_1 = 1$; $B'_2 = 1$) and aft antenna ($A' = -1$; $B'_1 = 1$; $B'_2 = 1$). After taking the opposite of the aft signal, and shifting it by 180°, a full 360° sample is obtained.

$$\delta\phi = D'_1 \frac{\cos\theta}{H}. \quad (36)$$

With an uncertainty in D'_1 on the order of 10 m, and for a flight altitude of 4000 m, the uncertainty in $\delta\phi$ would be about 0.15°.

2) ERROR IN THE AIRCRAFT ALTITUDE

The radio altimeter onboard the aircraft yields a measurement of altitude H with an accuracy of a few tens of meters. From the D'_2 in (35) we may write

$$\delta H = D'_2 \cos\theta. \quad (37)$$

Since D'_2 is itself determined within ± 10 m, this equation cannot help to improve the estimate of the radio altimeter.

3) ERROR IN THE HORIZONTAL VELOCITY

Two parameters characterize the bias in surface Doppler velocity: the drift angle α, and the aircraft horizontal ground speed V_H. The estimators for corresponding errors, drawn from A' and B'_1 in (35), are

$$\delta\alpha = \frac{\sin\alpha A'}{V_H \sin\theta} + \frac{\cos\alpha B'_1}{V_H \cos\theta} \quad (38)$$

$$\delta V_H = -\frac{\cos\alpha A'}{\sin\theta} + \frac{\sin\alpha B'_1}{\cos\theta} \quad (39)$$

A systematic error in α should be interpreted as a mounting error of the INS or antenna. To a good approximation, we may write

$$\langle \delta\alpha \rangle = \left\langle \frac{B_1'}{V_H \cos\theta} \right\rangle. \quad (40)$$

With an uncertainty of 0.1 m s^{-1} in A' and B_1', $\delta\alpha$ and δV_H may be determined within ±0.05° and ±0.3 m s^{-1}, respectively.

4) Errors in the pitch angle and in the vertical velocity

The biases in pitch angle ($\delta\beta$) and vertical velocity (δW) can be solved explicitly from the coefficients B_2' and C' in (35) as follows:

$$\delta\beta = \frac{C' \cos\theta}{H \tan\theta}$$

$$\delta W = \frac{B_2'}{\cos\theta} + \frac{C' V_H \cos\alpha \cos\theta}{H \tan\theta}. \quad (41)$$

However, with H = 4000 m, V_H = 120 m s^{-1}, θ = 30°, and uncertainties in C' and B_2' of ±10 m and ±0.1 m s^{-1}, respectively, these formulas lead to uncertainties in $\delta\beta$ and δW of ±0.35° and ±0.8 m s^{-1}, respectively. These uncertainties are much larger than the uncertainties embedded in the INS data as described in section 4a. This leads us to consider a variational approach that integrates first, our knowledge of the statistical uncertainties in C' and B_2', and second, the a priori knowledge that we have about the possible errors in W and β. Presumably, the main source of error does not lie in the navigation system, but in the possible mounting error of the pedestal, which may reach 1°.

Let $\sigma(B_2')$ and $\sigma(C')$ be the rms errors in B_2' and C', and $\sigma(W)$ and $\sigma(\beta)$ be the possible error in W and β. We may determine δW and $\delta\beta$ as the solution of the following variational problem:

$$\frac{(B_2' - \cos\theta\delta W + V_H \cos\alpha \cos\theta\delta\beta)^2}{\sigma^2(B_2')} + \frac{(C' - H\delta\beta \tan\theta/\cos\theta)^2}{\sigma^2(C')} \quad (42)$$

under the subsidiary condition that minimizes the following expression:

$$\frac{(\delta W)^2}{\sigma^2(W)} + \frac{(\delta\beta)^2}{\sigma^2(\delta\beta)}. \quad (43)$$

The solution of this variational problem is obtained by introducing a weak constraint and weighting function μ, and differentiating with respect to δW and $\delta\beta$ (see Courant and Hilbert 1953):

$$0 = \frac{V_H \cos\alpha \cos\theta(B_2' - \cos\theta\delta W + V_H \cos\alpha \cos\theta\delta\beta)}{\sigma^2(B_2')} - \frac{H \tan\theta}{\cos\theta} \frac{(C' - H\delta\beta \tan\theta/\cos\theta)}{\sigma^2(C')} + \frac{\mu\delta\beta}{\sigma^2(\beta)} \quad (44)$$

$$0 = -\frac{\cos\theta(B_2' - \cos\theta\delta W + V_H \cos\alpha \cos\theta\delta\beta)}{\sigma^2(B_2')} + \frac{\mu\delta W}{\sigma^2(W)}. \quad (45)$$

The solution of this set of linear equations (in appendix C) is

$$\delta\beta = \frac{1}{D}\left\{ -\frac{H \sin\theta C'}{\sigma^2(B_2')\sigma^2(C')} + \frac{\mu}{\sigma^2(W)}\left[\frac{V_H \cos\alpha \cos\theta B_2'}{\sigma^2(B_2')} - H\left(\frac{\tan\theta}{\cos\theta}\right)\frac{C'}{\sigma^2(C')} \right] \right\} \quad (46)$$

$$\delta W = \frac{1}{D}\left[-\frac{V_H \cos\alpha H \sin\theta C'}{\sigma^2(C')\sigma^2(B_2')} - \left(H\frac{\tan\theta}{\cos\theta}\right)^2 \frac{\cos\theta B_2'}{\sigma^2(C')\sigma^2(B_2')} - \frac{\mu \cos\theta B_2'}{\sigma^2(\beta)\sigma^2(B_2')} \right], \quad (47)$$

with

$$D = \left[\frac{(H \tan\theta/\cos\theta)^2}{\sigma^2(C')} + \frac{\mu}{\sigma^2(\beta)} \right] \frac{\cos^2\theta}{\sigma^2(B_2')} + \left[\frac{(V_H \cos\alpha \cos\theta)^2}{\sigma^2(B_2')} + \frac{(H \tan\theta/\cos\theta)^2}{\sigma^2(C')} + \frac{\mu}{\sigma^2(\beta)} \right] \frac{\mu}{\sigma^2(W)}. \quad (48)$$

The following values of the standard deviations may be introduced in the process: $\sigma(B_2')$ = 0.1 m s^{-1}, $\sigma(C')$ = 10 m, $\sigma(W)$ = 0.1 m s^{-1}, and $\sigma(\beta)$ = 0.05°.

7. Evaluation of the technique using TOGA COARE ELDORA/ASTRAIA data

The corrections to the navigation factors (e.g., pitch, drift, etc.) were evaluated using radar data from 14 periods (Table 1) that included samples from the ELDORA/ASTRAIA flights from five days of research in February 1993 during the Tropical Ocean Global Atmosphere Coupled Ocean–Atmosphere Response Experiment (TOGA COARE). Each of the 14 periods included a number of scans, typically between 17 and 50 full 360° scans. The results are very consistent among all 14 periods. As

TABLE 1. ELDORA correction factor evaluation. The correction factors are evaluated for two or more groups of scans on five flights in February 1993. Each group of scans contains 17 or more individual scans.

Date	Time (UTC)	Scans	ΔR_f (m)	ΔR_a (m)	$\delta\beta$ (°)	$\delta\alpha$ (°)	$\delta\phi$ (°)	δH (m)	δV_H (m s^{-1})
6 Feb 93	1847–1857	50	22	16	−1.44	−0.19	2.29	−10	0.5
6 Feb 93[a]	1948–1958	50	100	90	−1.46	0.61	1.26	50	−1.4
9 Feb 93	1608–1618	25	17	−10	−1.43	−1.12	2.41	−10	−0.63
9 Feb 93	1834–1843	25	7	11	−1.30	−1.84	2.23	−10	−2.19
9 Feb 93[b]	1940–1950	25	0	6	−1.33	0.21	2.33	−10	−0.85
10 Feb 93	1846–1901	80	3	−9	−1.42	−1.09	2.32	20	−0.88
10 Feb 93[c]	2037–2052	25	10	1	−1.43	−0.49	1.26	10	−0.63
10 Feb 93	2053–2058	25	10	11	−1.43	−0.51	2.34	0	−0.51
10 Feb 93[d]	2306–2312	25	33	9	−1.42	−0.37	2.39	10	−0.13
17 Feb 93	2008–2014	26	48	17	−1.48	−0.81	2.40	10	1.2
17 Feb 93	2030–2040	29	30	10	−1.48	−0.1	2.37	0	0.85
17 Feb 93	2219–2229	50	80	67	−1.45	−0.88	2.30	40	−0.45
18 Feb 93	2129–2139	52	25	−10	−1.47	−1.0	2.31	−10	−0.68
18 Feb 93	0100–0103	17	50	35	−1.46	−1.35	2.30	20	−1.17
Mean values			31	17	−1.43	−0.64	2.18	7.8	−0.50

[a] Variable corrections between 1952 and 1956 UTC.
[b] Aircraft turn and variable corrections around 1943 UTC.
[c] First file of tape: subsequent files have different corrections.
[d] Aircraft climbing. Heading changes smoothly from 360° to 180°.

an example, the results from 2128:00 to 2139:00 UTC 18 February 1993 are presented in this section.

A subset of the flight parameters during this time period is illustrated in Fig. 6. In this time period, the aircraft was moving toward 357° at the 4820-m altitude with a steady pitch angle. The drift angle steadily decreases from 2.5° to 1° while the aircraft vertical velocity varied between −0.4 and 0.4 m s^{-1}. The circles in Fig. 6 and subsequent figures indicate the original values of each parameters while pluses indicate the corresponding values after the procedure outlined in section 3 is applied (normally three to four iterations).

The curve fits using the original data from only fore and aft-radar (180° data) are illustrated in Figs. 7 and 8, while the curve fits from combining data from fore and aft radars (360° data) are shown in Fig. 9. As discussed in the previous section, the curve fits using data from only one radar are subject to large uncertainties due to the limited data in the ϕ domain. This can be illustrated by comparing the fitted curve of the velocity residual among Figs. 7–9. The curves in Figs. 7 and 8 are similar but the amplitude in Fig. 8 has 1 m s^{-1} difference as compared with the curve in Fig. 9. The range delay (coefficient E) and the tilt angle corrections from fore and aft radars are also shown in Figs. 7 and 8. The procedure converged after four iterations. The net corrections after each iteration are listed in Table 2.[3] The convergence criteria based on the intrinsic accuracy of individual measurements are listed in Table 3. The goodness of the curve fit can be also determined from the $\sigma(\delta R_G)$ and $\sigma(\delta V_G)$. The iterative process should cease when $\sigma(\delta R_G)$ and $\sigma(\delta V_G)$ stop decreasing. These values will be used to obtain A', B'_1, B'_2, C', D'_1, and D'_2 while E is forced to be zero in this process. The resulting coefficients are shown in Fig. 10.

The sea surface reflectivity factor, velocity, and range residual from an original scan (Fig. 9) can be seen to vary considerably as the radar scans and the spin angle ϕ changes. The points (+) are the range and velocity residual of the ground gates selected using the procedure outlined in section 3. The smooth curves (composed by circles) are the least-squares curve fit to the data points. The reflectivity data (top panel) do not change except that they are shifted by the spin angle correction between the corrected and uncorrected data. The velocity residual (left middle panel) shows that in the original data the ocean surface moved at an estimated speed of approximately 4 m s^{-1} in a large portion of a scan. As a result, the Doppler velocity bias can be expected to have the

[3] The range delay of −320 m is obtained after the first iteration of the procedure. Since the range delay recorded on the ELDORA tape header was 440 m, the net range delay is 10 m in agreement with that in Table 1.

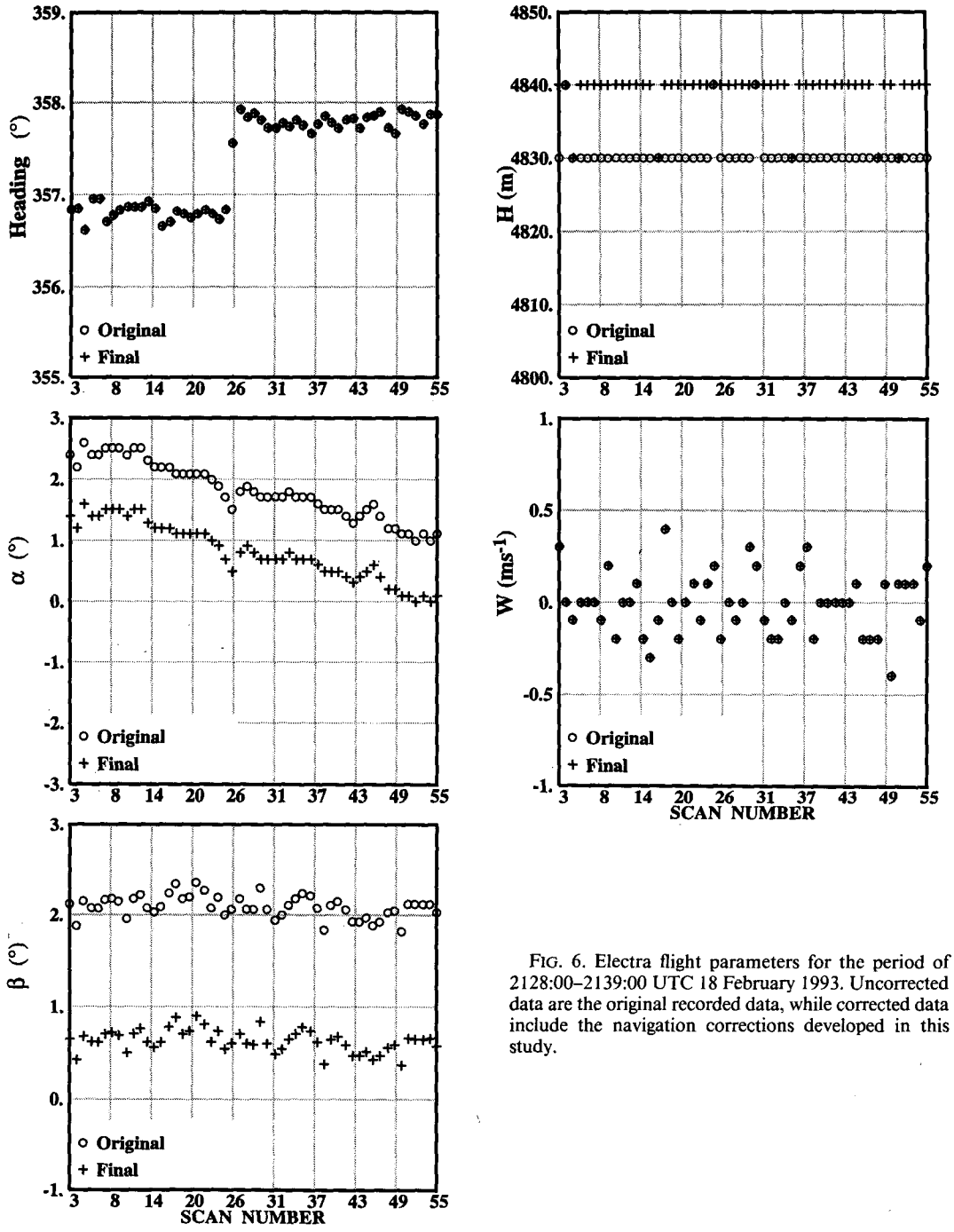

FIG. 6. Electra flight parameters for the period of 2128:00–2139:00 UTC 18 February 1993. Uncorrected data are the original recorded data, while corrected data include the navigation corrections developed in this study.

same magnitude as the velocity residual from the return of the ocean surface and, most importantly, this Doppler velocity bias varies as the radar spin angle changes. A similar situation exists in the range residual (bottom panel) where the original range bias varies with the spin angle and the magnitude can exceed 400 m. These nonconstant biases can create false convergence in the synthesized wind fields and ultimately affect the accuracy of the subsequently derived quantities.

The purpose of this procedure is to identify the error sources and bring the velocity and range residues as close to zero as possible. The velocity and range residues improved after the data were corrected for the navigation and radar mounting bias after four iterations through

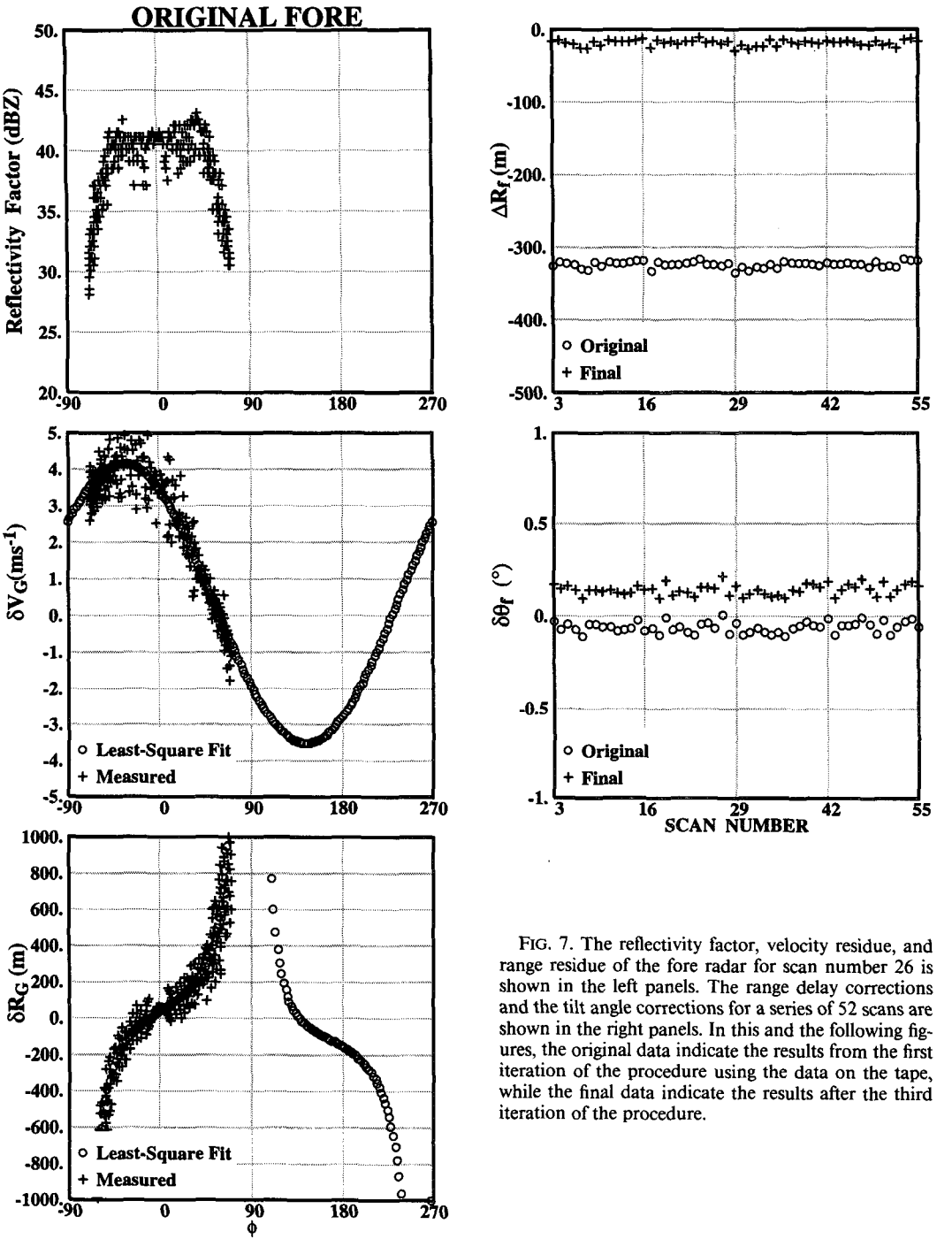

FIG. 7. The reflectivity factor, velocity residue, and range residue of the fore radar for scan number 26 is shown in the left panels. The range delay corrections and the tilt angle corrections for a series of 52 scans are shown in the right panels. In this and the following figures, the original data indicate the results from the first iteration of the procedure using the data on the tape, while the final data indicate the results after the third iteration of the procedure.

the procedure. The magnitude of the fitted velocity residual is near zero with a standard deviation of about 0.5 m s^{-1} and the magnitude of the range residual is also near zero with a standard deviation of about 60 m. The extreme values near 90° and 270° are the singularities of the cosine square factor in (18).

Based on the A', B'_1, B'_2, C', D'_1, and D'_2 coefficients (Fig. 10), we can evaluate corrections to the rotation angle, aircraft altitude, drift, horizontal velocity, pitch,

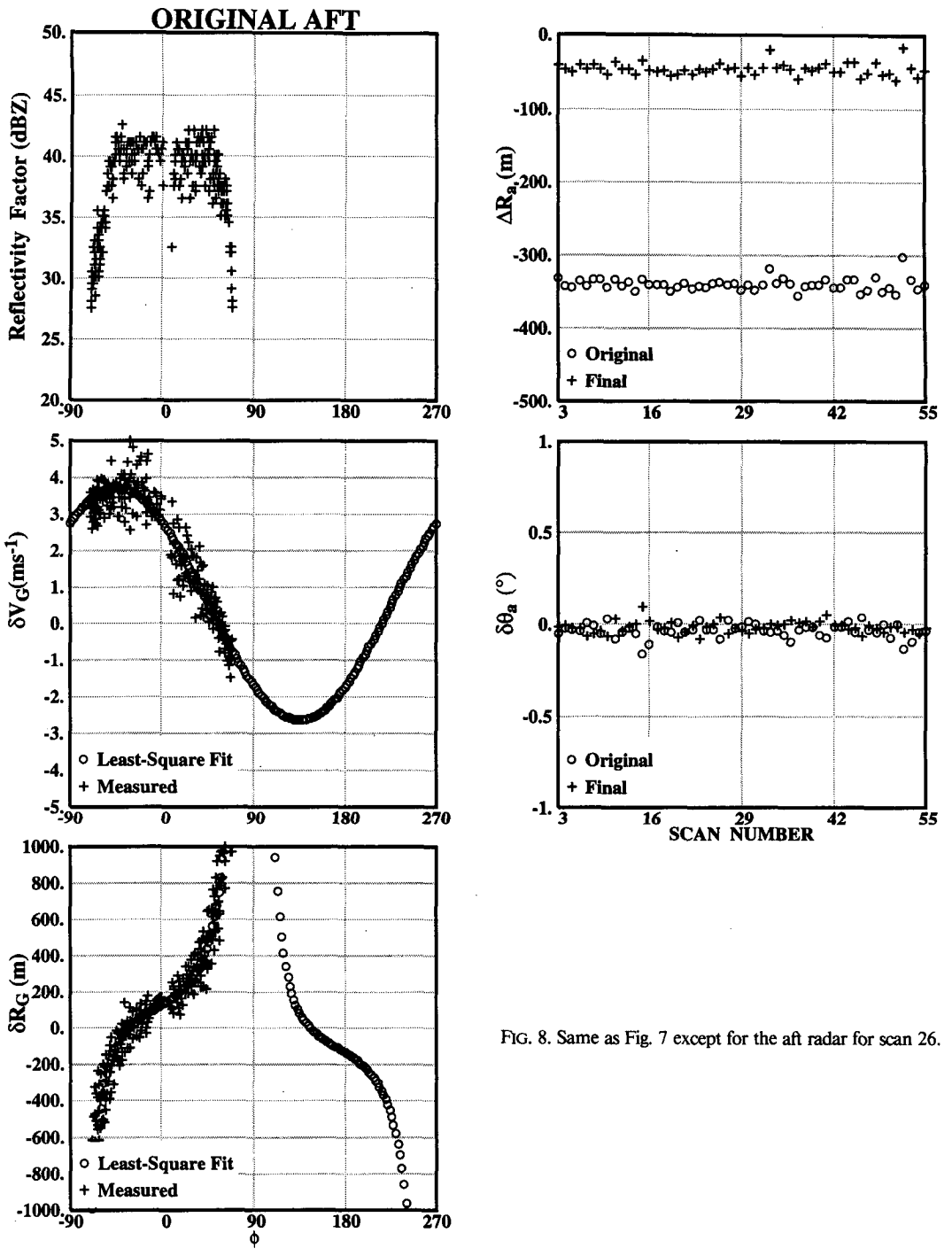

FIG. 8. Same as Fig. 7 except for the aft radar for scan 26.

and aircraft vertical velocity [(36)–(39), (46), and (47)] for each individual scan. These resulting correction factors for a series of 52 scans (2129–2139 UTC 18 February 1993) are shown in Fig. 11. (The data displayed in Figs. 7–9 are scan number 26 in this series.)

The correction factors in the range to the first gate (range delay ΔR) for the fore and aft radars were nearly constant for all time periods reviewed. The variability in the range delay error is considerably less than half of a gate length (75 m during TOGA COARE), which is the upper limit of the uncertainty in range residual. This is also consistent with the mean standard deviation of the range residual ($\approx$60 m) after the corrections are applied to the dataset. There is essentially no difference

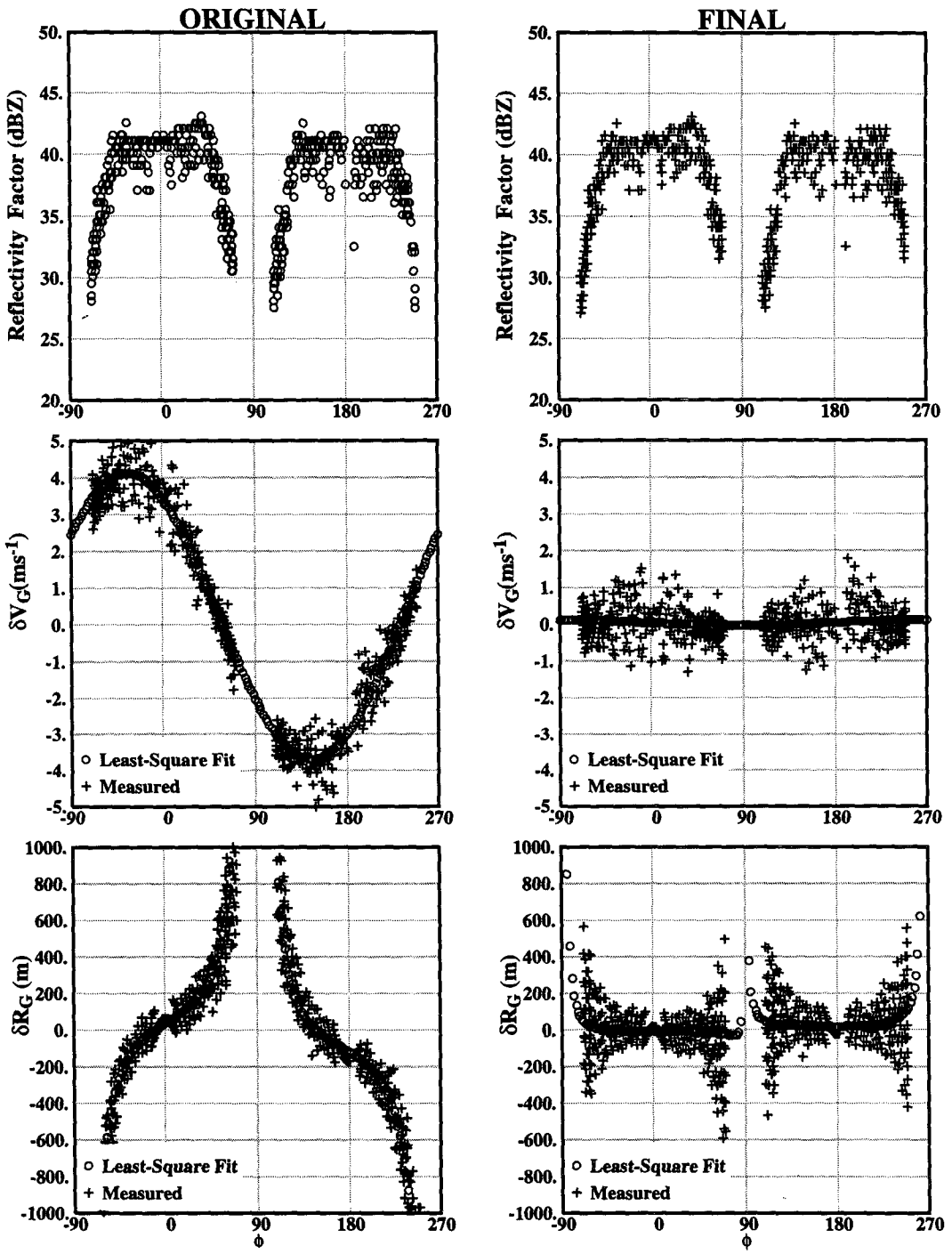

FIG. 9. The reflectivity factor (top panel), velocity residue (middle panel), and range residue (bottom panel) of the potential ground gates selected by the procedure described in section 2. Original data are the data recorded on the tape while final data are reprocessed using the new navigation information obtained in this study after four iterations.

in range delay between the fore and aft radars in the ELDORA system. The pitch and rotation angle also have stable biases that are within expectations. The most unstable parameter is the drift bias, which, due to the measurement error in the heading, can vary by about ±1°. The measured drift bias variability of approximately 0.64° is consistent with this expected measurement error. This drift bias variability should

TABLE 2. Correction factors for 2129–2139 UTC 18 February 1993. Values shown are the best estimates of the net correction factors after each iteration.

No. iter.	ΔR_f (m)	ΔR_a (m)	δH (m)	δV_H (m s^{-1})	$\delta\alpha$ (°)	$\delta\beta$ (°)	$\delta\phi$ (°)	$\sigma(\delta R_G)$ (m)	$\sigma(\delta V_G)$ (m s^{-1})
1	110	94	70	−0.45	−1.0	−1.50	2.21	100	0.37
2	84	43	30	−0.61	−1.0	−1.47	2.29	61	0.38
3	44	14	10	−0.66	−1.0	−1.47	2.31	58	0.40
4	25	−11	−10	−0.68	−1.0	−1.47	2.31	63	0.47

be expected to introduce variable errors in the aircraft horizontal velocity of about 1 m s^{-1}, which is again consistent with the aircraft horizontal ground speed corrections in Table 1. The flight-to-flight deviations among all other parameters are negligible except for the aircraft pressure altitude, where day-to-day variations are expected due to the deviation in surface pressure and the lapse rate from the standard atmosphere (List 1984). During TOGA COARE, the aircraft altitude obtained from the radio altimeter aboard the Electra was used whenever was available. This drastically reduces the large uncertainties in aircraft altitude that are introduced if the pressure altitude is used; at 4600-m pressure altitude, the error can be as large as 200 m.

Inspection of the values from this and other data samples shows that there is generally little variability from scan to scan or from day to day. Those cases that have significant variability generally include some abrupt or frequently changing aircraft motion that basically violates the underlying assumptions of this technique. Even after there are some perturbations in the values of the coefficients, they typically settle back to the same stable values. This suggests 1) the possibility of using a single set of corrections for all the data, and 2) that these temporary perturbations in the coefficient values may be related to instrumentation issues such as time lags between measurements made by different instruments.

This analysis indicates that a single set of corrections for the entire TOGA COARE ELDORA dataset should account for most errors in navigation of the data except for the drift and aircraft ground speed biases. These correction factors are 2.3° for rotation angle, −1.45° for pitch, 8 m for the aircraft altitude, and 30 m for the range delay. After these corrections are applied to the data, only small residual errors remain (see the final data in Fig. 9). These small residual errors can be removed using more detailed scan-by-scan corrections if the analysis warrants.

For most analysis purposes this is generally unnecessary, since the mean residual range error is at most 20–40 m and the mean residual velocity error is less than or equal to 0.5 m s^{-1}. Reevaluation of the coefficients, shown in Fig. 9, indicates that considerably smaller values with less scatter result. Tests of further corrections to the data indicate that additional reductions to the errors do not result from reapplication of this process after three to four iterations.

Figure 12 shows comparisons of the velocity scans from the ELDORA/ASTRAIA radar, before and after the data renavigation process is completed. In these pictures, the aircraft is flying into the page at an altitude of about 4 km at the center of the range rings. In the uncorrected reflectivity data (top) the sea surface can be seen to be slightly rotated counterclockwise from the correct position that can be seen in the renavigated (lower) data. While these corrections are subtle, they are critical to bringing the data to a quality where analyses can be made with minimal concern for editing.

8. Summary and conclusions

A procedure to determine the navigation biases using the radar returns from the flat earth surface is presented in this paper. It has been shown that the surface return, which has been considered as clutter to the meteorological data, can be used to estimate the INS navigation biases and the radar pointing and ranging biases. Using a least-squares curve fit on the range and velocity residual of the surface echo, a total of eight biases (drift, pitch, spin angle, tilt, range delay, aircraft ground speed, aircraft vertical velocity, and aircraft altitude) can be estimated objectively. As a test, this procedure was applied to a total of 14 individual time periods of ELDORA/ASTRAIA data collected during the TOGA COARE experiment. These results indicate that these biases are stable from flight-to-flight except for the drift and aircraft ground speed biases. These small biases can produce a-few-

TABLE 3. Convergence criteria for individual parameters used in the iterative procedure.

	ΔR_f (m)	ΔR_a (m)	δH (m)	δV_H (m s^{-1})	$\delta\alpha$ (°)	$\delta\beta$ (°)	$\delta\phi$ (°)
Convergence criteria	20	20	20	0.1	0.1	0.1	0.1

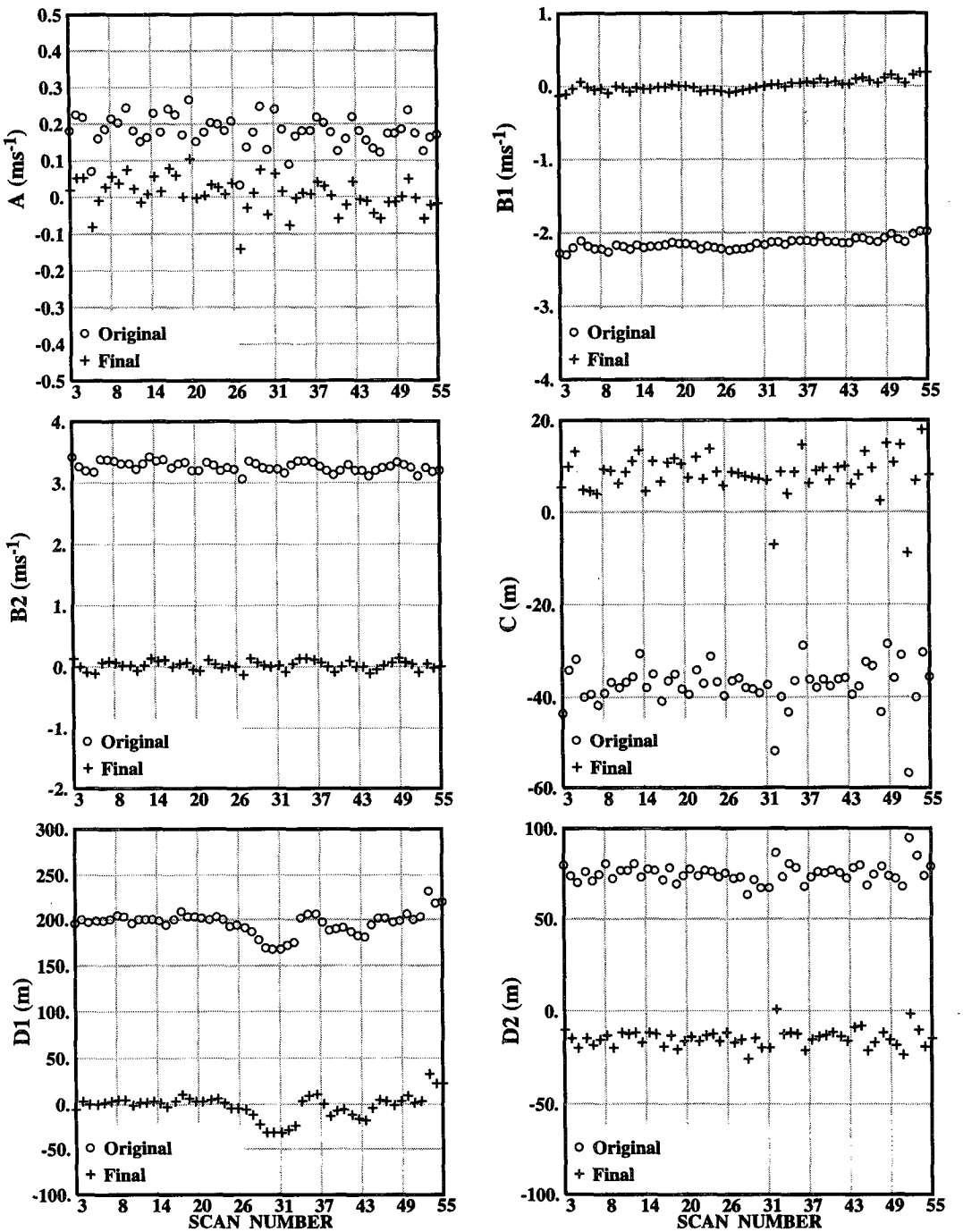

FIG. 10. The scan-by-scan coefficients of A, B_1, B_2, C, D_1, D_2, and E. Uncorrected coefficients are obtained from the least-squares fit using the original data, while corrected coefficients are obtained using the renavigated data. The corrections labeled "original" are obtained from the first iteration of the procedure. The corrections labeled "final" are obtained after applying the cumulative corrections (four iterations) to the original data. These near-zero values indicate that no additional corrections are needed.

meter-per-second errors in the measured Doppler velocities. Removing these velocity errors is critical to obtain accurate vertical velocities and other flux calculations. Fortunately, these biases can be identified and corrected objectively using the procedure described in this paper.

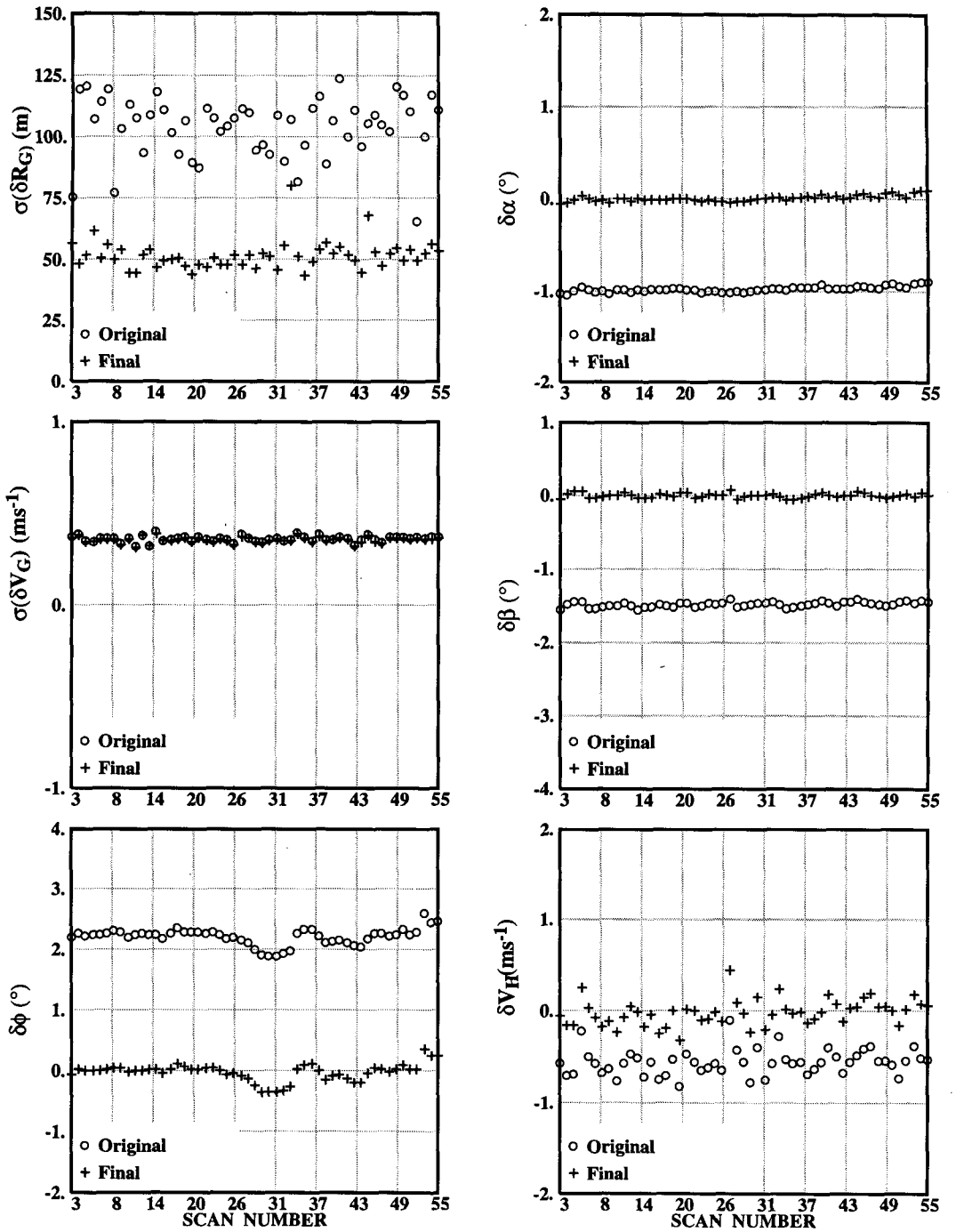

FIG. 11. The scan-by-scan plot of the corrections computed from the coefficients illustrated in Fig. 9. The uncorrected data show the amount needed to correct for each parameter after the first iteration. The corrected data show the required corrections after four iterations.

A few recommendations regarding data collection and using this technique are provided in the following:

• This procedure is designed to process data collected during a steady flight leg. During three of the 14 time periods, there were interscan variations in the correction factors due to heading change and pitch change that require additional corrections to the radial velocities. These additional corrections are discussed by Lee et al. (1994) and

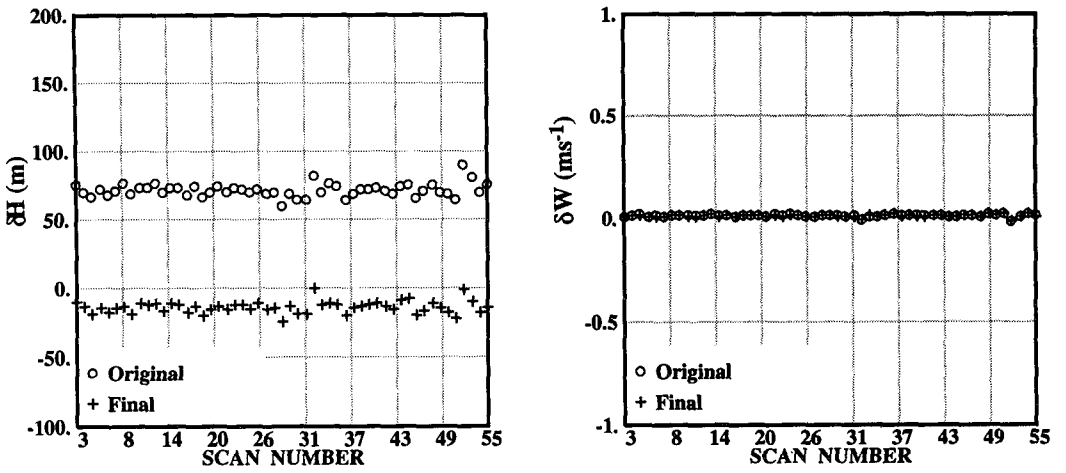

FIG. 11. (*Continued*)

the implementation is beyond the scope of this paper.

- Users of this technique are advised to interpret any correction factors in the immediate stormy environment with caution because 1) the earth surface finding procedure, which looks for high reflectivity and near-zero velocities independently, can be biased by the presence of storms, and 2) the flight parameters can become unsteady within a scan while encountering strong turbulence.
- During the TOGA COARE experiment, the majority of data collected by the ELDORA/ASTRAIA is 180° scans (i.e., the radar scans on only one side of the aircraft). The correction factors obtained from these 180° scans are usually unstable (not shown) for the reasons described in section 5. We therefore recommend that the correction factors should always be computed using data from 360° scans.
- As illustrated in this paper, most of the correction factors are stable throughout a flight and from flight to flight. Therefore, these corrections can be used as a template to correct the data collected in 180° scan mode. Then the remaining uncertainties (most likely drift and aircraft ground speed) can be dealt with separately as required. We strongly recommend users to examine their data after these correction factors are applied to ensure data quality for the multi-Doppler radar analysis.
- Due to the 2° beamwidth, the usable sector of data within a scan for the surface echo calculation decreases rapidly with decreasing aircraft altitude. Similarly, the accuracy of $\delta\phi$ decreases as the aircraft altitude decreases [Eq. (36)]. The desired aircraft altitude for the surface echo calculation is anywhere above 3 km above the surface. We do not recommend performing the surface echo calculation when the aircraft altitude is lower than 500 m above surface.

Specific recommendations on how to properly collect and analyze the earth surface return are also made. In the future, we plan to implement this procedure in real time in the air so as to identify these biases while the data are collected. Obtaining the correction factors in real time will expedite the process of delivering data to the user in the future.

Acknowledgments. The authors would like to thank Sherrie Daud, Jeremy Hackney, and Susan Stringer for their assistance in coding, debugging, and testing of the program. The reviews by Peter Dodge, Eastwood Im, Frank Marks, and Tomas Matejka, significantly improved this manuscript. Illustrations provided by NCAR Graphics are greatly appreciated. Ann-Elizabeth Nash proofread this manuscript.

APPENDIX A

Derivation of Angles Ψ, EL, and A_z

Recall the formulas of spherical trigonometry: A, B, and C are the angles at corners of a spherical triangle whose opposite arcs are a, b, and c (all parameters in radians). These parameters are related through the basic equations from the law of sine and the law of cosine:

$$\frac{\sin a}{\sin A} = \frac{\sin b}{\sin B} = \frac{\sin c}{\sin C}$$

$$\cos a = \cos b \cos c + \sin b \sin c \cos A$$

$$\cos A = -\cos B \cos C + \sin B \sin C \cos a.$$

These basic equations are applied successively in the following spherical triangles of Fig. 2a. As a result of the definition we obtain

arc $CD = \pi/2$,
arc $BC = \beta$ (pitch),

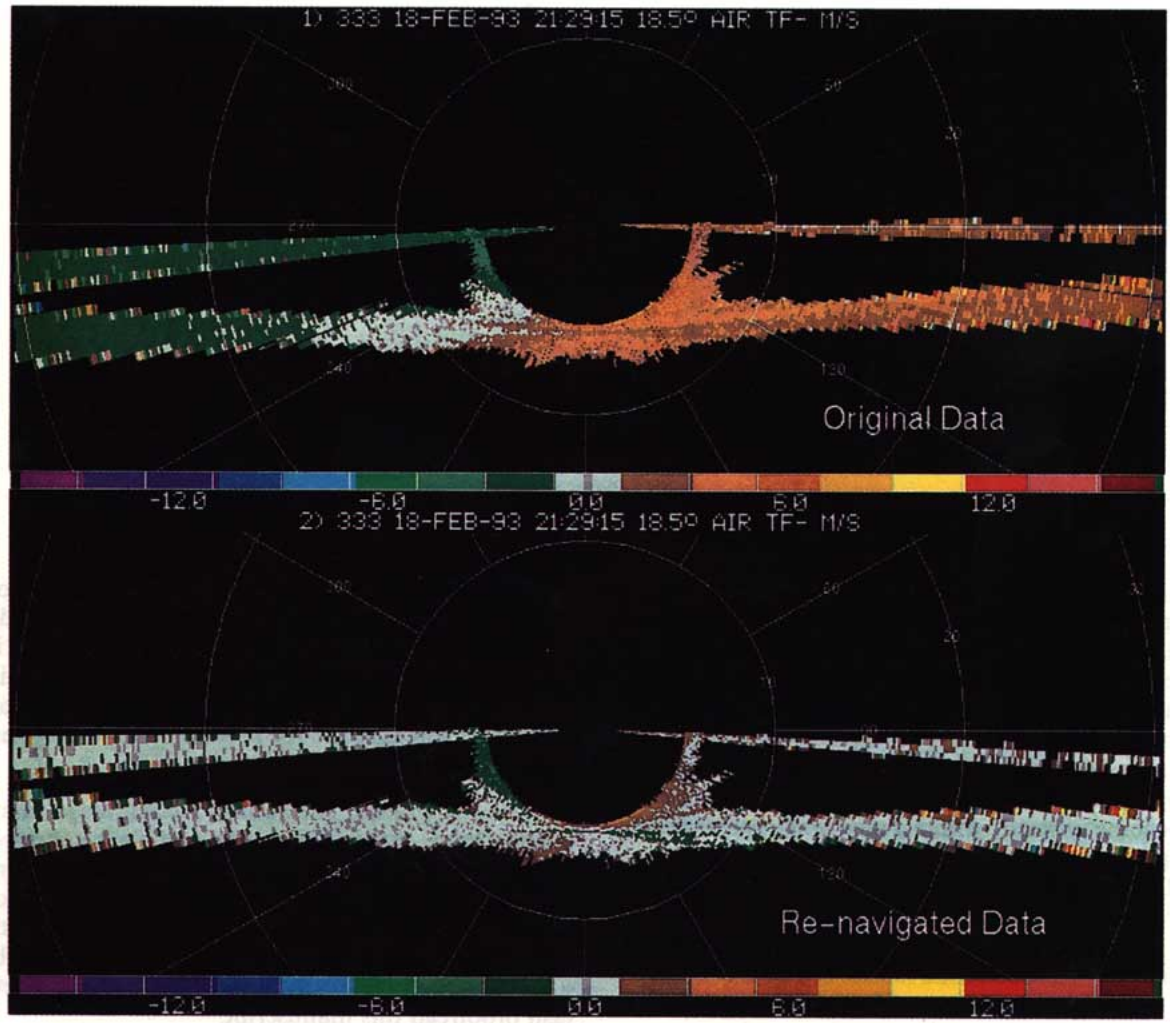

FIG. 12. Comparisons of the velocity scans from the ELDORA/ASTRAIA radar, before and after the data renavigation process is completed. In these pictures, the aircraft is flying into the page at an altitude of about 4 km, at the center of the 10-km range rings. The beams extended from both sides of the aircraft are second trip sea clutters. The sea surface is the narrow horizontal band whose velocities were between −3 and +3 m s^{-1} in the original data (upper panel) and were near zero after the data were renavigated.

arc $AB = \alpha$ (drift),
arc $ED = \theta$ (airframe-relative tilt angle),
arc $EA = \Psi(\pi/2$ minus track-relative tilt angle),
arc $EF =$ EL (earth-relative elevation angle),
arc $BF = A_z$ (track-relative azimuth angle).

The parameters of interest are Ψ, EL, and A_z.

To derive EL and A_z, we can use the triangle ZEC, where

arc $ZE = \pi/2 - \text{EL}$,
arc $CE = \pi/2 - \theta$,
arc $CZ = \pi/2 - \beta$,
angle $ZCE = \phi - \pi$,
angle $CZE = A_z$.

Then from the law of cosines, EL can be obtained:

$$\sin\text{EL} = \sin\theta \sin\beta - \cos\theta \cos\beta \cos\phi \quad \text{(A1)}$$

and A_z can be obtained:

$$\sin\theta = \sin\text{EL} \sin\beta + \cos\text{EL} \cos\beta \cos A_z$$

or

$$\cos A_z = \frac{\sin\theta - \sin\text{EL} \sin\beta}{\cos\text{EL} \cos\beta}.$$

To derive Ψ, we start from triangle ABE, where

arc $AE = \Psi$,
arc $AB = \alpha$,
$\cos\Psi = \cos\alpha \cos BE + \sin\alpha \sin BE \cos ABE$.

To obtain $\cos BE$, we use triangle BCE, where

arc $BC = \beta$,
arc $EC = \pi/2 - \theta$,
angle $BCE = \phi$.

Then, from the law of cosines:

$$\cos BE = \cos\beta \sin\theta + \sin\beta \cos\theta \cos\phi \quad \text{(A2)}$$

and from the law of sines:

$$\frac{\cos\theta}{\sin EBC} = \frac{\sin BE}{\sin\phi}; \quad \text{(A3)}$$

also angle $ABE = \pi/2 +$ angle CBE, therefore, $\cos ABE = -\sin CBE$. Then, we have

$$\cos\Psi = \cos\alpha \cos\beta \sin\theta + \cos\alpha \sin\beta \cos\theta \cos\phi - \sin\alpha \cos\theta \sin\phi. \quad \text{(A4)}$$

APPENDIX B

Derivation of C, D_1, D_2, and E

The quadratic form (26) to be minimized is

$$Q = \sum_{\{i\}} [\cos^2\phi_i (R_R - R_{Ge})_i - C - D_1 \sin\phi_i - D_2 \cos\phi_i - E \cos 2\phi_i]^2 + \mu N (C^2 + D_2^2 + E^2). \quad \text{(B1)}$$

Consequently C, D_1, D_2, and E should verify

$$\frac{\partial Q}{\partial C} = 0, \quad \frac{\partial Q}{\partial D_1} = 0, \quad \frac{\partial Q}{\partial D_2} = 0, \quad \frac{\partial Q}{\partial E} = 0, \quad \text{(B2)}$$

or

$$N(1+\mu)C + \left(\sum_{\{i\}} \sin\phi_1\right) D_1 + \left(\sum_{\{i\}} \cos\phi_i\right) D_2 + \left(\sum_{\{i\}} \cos 2\phi_i\right) E = \sum_{\{i\}} \cos^2\phi_i (R_R - R_{Ge})_i \quad \text{(B3)}$$

$$\left(\sum_{\{i\}} \sin\phi_i\right) C + \left(\sum_{\{i\}} \sin^2\phi_i\right) D_1 + \left(\sum_{\{i\}} \sin\phi_i \cos\phi_i\right) D_2 + \left(\sum_{\{i\}} \sin\phi_i \cos 2\phi_i\right) E = \sum_{\{i\}} \cos^2\phi_i (R_R - R_{Ge})_i \sin\phi_i \quad \text{(B4)}$$

$$\left(\sum_{\{i\}} \cos\phi_i\right) C + \left(\sum_{\{i\}} \sin\phi_i \cos\phi_i\right) D_1 + \left[\left(\sum_{\{i\}} \cos^2\phi_i\right) + N\mu\right] D_2 + \left(\sum_{\{i\}} \cos\phi_i \cos 2\phi_i\right) E = \sum_{\{i\}} \cos^2\phi_i (R_R - R_{Ge})_i \cos\phi_i \quad \text{(B5)}$$

$$\left(\sum_{\{i\}} \cos 2\phi_i\right) C + \left(\sum_{\{i\}} \sin\phi_i \cos 2\phi_i\right) D_1 + \left(\sum_{\{i\}} \cos\phi_i \cos 2\phi_i\right) D_2 + \left[\left(\sum_{\{i\}} \cos^2 2\phi_i\right) + N\mu\right] E = \sum_{\{i\}} \cos^2\phi_i (R_R - R_{Ge})_i \cos 2\phi_i. \quad \text{(B6)}$$

Standard numerical methods may now be used to solve this system for C, D_1, D_2, and E.

APPENDIX C

Derivation of $\delta\beta$ and δW

The matrix form of (44) and (45) is

$$\begin{pmatrix} M_{11} & M_{12} \\ M_{21} & M_{22} \end{pmatrix} \begin{pmatrix} \delta\beta \\ \delta W \end{pmatrix} = \begin{pmatrix} S_1 \\ S_2 \end{pmatrix}, \quad \text{(C1)}$$

with

$$M_{11} = \frac{(V_H \cos\alpha \cos\theta)^2}{\sigma^2(B_2')} + \frac{(H \tan\theta/\cos\theta)^2}{\sigma^2(C')} + \frac{\mu}{\sigma^2(\beta)}$$

$$M_{12} = -\frac{V_H \cos\alpha \cos^2\theta}{\sigma^2(B_2')}$$

$$M_{21} = -\frac{V_H \cos\alpha \cos^2\theta}{\sigma^2(B_2')}$$

$$M_{22} = \frac{\cos^2\theta}{\sigma^2(B_2')} + \frac{\mu}{\sigma^2(W)}$$

$$S_1 = \frac{V_H \cos\alpha \cos\theta B_2'}{\sigma^2(B_2')} - \frac{H(\tan\theta/\cos\theta)C'}{\sigma^2(C')}$$

$$S_2 = -\frac{\cos\theta B_2'}{\sigma^2(B_2')}.$$

The matrix determinant is

$$D = \left[\frac{(H \tan\theta/\cos\theta)^2}{\sigma^2(C')} + \frac{\mu}{\sigma(\beta)}\right] \frac{\cos^2\theta}{\sigma^2(B_2')} + \left[\frac{(V_H \cos\alpha \cos\theta)^2}{\sigma^2(B_2')} + \frac{(H \tan\theta/\cos\theta)^2}{\sigma^2(C')} + \frac{\mu}{\sigma^2(\beta)}\right] \frac{\mu}{\sigma^2(W)}.$$

The inverted matrix $\mathbf{M}^{-1}$ is defined by

$$M_{11}^{-1} = \frac{1}{D}\left[\frac{\cos^2\theta}{\sigma^2(B_2')} + \frac{\mu}{\sigma^2(W)}\right]$$

$$M_{12}^{-1} = \frac{1}{D}\left[\frac{V_H \cos\alpha \cos^2\theta}{\sigma^2(B_2')}\right]$$

$$M_{22}^{-1} = \frac{1}{D}\left[\frac{V_H \cos\alpha \cos^2\theta}{\sigma^2(B_2')}\right]$$

$$M_{21}^{-1} = \frac{1}{D}\left[\frac{(V_H \cos\alpha \cos\theta)^2}{\sigma(B_2')} + \frac{(H \tan\theta/\cos\theta)^2}{\sigma^2(C')} + \frac{\mu}{\sigma^2(\beta)}\right].$$

It follows that

$$\delta\beta = \frac{1}{D}\left\{-\frac{H\sin\theta C'}{\sigma^2(B_2')\sigma^2(C')} + \frac{\mu}{\sigma^2(W)} \times\left[\frac{V_H\cos\alpha\cos\theta B_2'}{\sigma^2(B_2')} - \frac{H(\tan\theta/\cos\theta)C'}{\sigma^2(C')}\right]\right\}$$

$$\delta W = \frac{1}{D}\left[-\frac{V_H\cos\alpha H\sin\theta C'}{\sigma^2(C')\sigma^2(B_2')} - \left(H\frac{\tan\theta}{\cos\theta}\right)^2\frac{\cos\theta B_2'}{\sigma^2(C')\sigma^2(B_2')} - \frac{\mu\cos\theta B_2'}{\sigma^2(\beta)\sigma^2(B_2')}\right].$$

REFERENCES

Courant, R., and D. Hilbert, 1953: *Methods of Mathematical Physics.* Interscience, 561 pp.

Hildebrand, P. H., and R. K. Moore, 1990: Meteorological radar observations from moving platforms. *Radar in Meteorology,* D. Atlas, Ed., Amer. Meteor. Soc., 287–315.

——, C. A. Walther, C. Frush, J. Testud, and G. Baudin, 1994: The ELDORA/ASTRAIA airborne Doppler weather radar. *IEEE,* **82,** 1873–1890.

Jorgensen, D. P., and J. D. DuGranrut, 1991: A dual-beam technique for deriving wind fields from airborne Doppler radar. Preprints, *25th Int. Conf. on Radar Meteorology,* Paris, France, Amer. Meteor. Soc., 458–461.

Lee, W.-C., P. Dodge, F. D. Marks, and P. H. Hildebrand, 1994: Mapping of airborne Doppler radar data. *J. Atmos. Oceanic Technol.,* **11,** 572–578.

List, R. J., 1984: *Smithsonian Meteorological Tables.* 5th ed., Smithsonian Institution, 527 pp.